

Orbital migration of giant planets induced by gravitationally unstable gaps: the effect of planet mass

Ryan Cloutier ^{*} and Min-Kai Lin [†]

Canadian Institute for Theoretical Astrophysics, 60 St. George Street, Toronto, ON, M5S 3H8, Canada

8 October 2018

ABSTRACT

It has been established that self-gravitating disc-satellite interaction can lead to the formation of a gravitationally unstable gap. Such an instability may significantly affect the orbital migration of gap-opening perturbers in self-gravitating discs. In this paper, we extend the two-dimensional hydrodynamic simulations of Lin & Papaloizou to investigate the role of the perturber or planet mass on the gravitational stability of gaps and its impact on orbital migration. We consider giant planets with planet-to-star mass ratio $q \equiv M_p/M_* \in [0.3, 3.0] \times 10^{-3}$ (so that $q = 10^{-3}$ corresponds to a Jupiter mass planet if $M_* = M_\odot$), in a self-gravitating disc with disc-to-star mass ratio $M_d/M_* = 0.08$, aspect ratio $h = 0.05$, and Keplerian Toomre parameter $Q_{k0} = 1.5$ at 2.5 times the planet’s initial orbital radius. These planet masses correspond to $\tilde{q} \in [0.9, 1.7]$, where \tilde{q} is the ratio of the planet Hill radius to the local disc scale-height. Fixed-orbit simulations show that all planet masses we consider open gravitationally unstable gaps, but the instability is stronger and develops sooner with increasing planet mass. The disc-on-planet torques typically become more positive with increasing planet mass. In freely-migrating simulations, we observe faster outward migration with increasing planet mass, but only for planet masses capable of opening unstable gaps early on. For $q = 0.0003$ ($\tilde{q} = 0.9$), the planet undergoes rapid inward type III migration before it can open a gap. For $q = 0.0013$ ($\tilde{q} = 1.5$) we find it is possible to balance the tendency for inward migration by the positive torques due to an unstable gap, but only for a few 10^3 ’s of orbital periods. We find the unstable outer gap edge can trigger outward type III migration, sending the planet to twice its initial orbital radius on dynamical timescales. We briefly discuss the importance of our results in the context of giant planet formation on wide orbits through disc fragmentation.

Key words: planetary systems: formation, planetary migration, protoplanetary discs

1 INTRODUCTION

From the discovery of ‘hot Jupiters’ (e.g. 51 Peg b, Mayor & Queloz 1995) to long-period giant planets (e.g. HR 8799b, Marois et al. 2008), the wide range of observed exoplanet orbital radii suggest that orbital migration due to gaseous disc-satellite interaction may play an important role in planet formation theory. Since its initial development (Goldreich & Tremaine 1979, 1980), disc-satellite interaction has been studied with the inclusion of increasingly complex physics. For a review of the theory and recent advancements, see Kley & Nelson (2012) and Baruteau & Masset (2013).

A less well-explored area is the interaction between a planet and large-scale instabilities in the disc. For example, recent works have shown that disc gaps induced by a planet can be dynamically unstable under appropriate conditions (Koller et al. 2003; Li et al. 2005; Lin & Papaloizou 2010, 2011b). Gap-opening requires a sufficiently massive planet (Lin & Papaloizou 1986) and/or low viscosity disc (Rafikov 2002; Dong et al. 2011; Duffell & MacFadyen 2013).

In a self-gravitating disc, planet gaps may become gravitationally unstable (Meschiari & Laughlin 2008; Lin 2012b) even if the initial disc is Toomre stable (Toomre 1964). The result of this instability is the development of large-scale spiral arms associated with the gap edge, which exert significant torques on the planet (Lin & Papaloizou 2011a). This gravitational edge instability, and its impact on orbital migration, has been less appreciated. However, it may be rele-

^{*} E-mail: cloutier@cita.utoronto.ca

[†] E-mail: mklin924@cita.utoronto.ca

vant to planet formation theories requiring a self-gravitating disc (e.g., Boss 1997; Nayakshin 2010, 2013). We remark that in the ‘tidal downsizing’ theory, Nayakshin discusses gap-opening in massive discs, a situation that we consider in this work.

In a previous study, Lin & Papaloizou (2012, hereafter LP12) simulated the orbital migration of a gap-opening giant planet in self-gravitating discs which became gravitationally unstable only in the presence of a planet gap. They found a gravitationally unstable outer gap edge induced *outward* orbital migration.

LP12 fixed the planet mass in their simulations. However, since the instability is associated with the gap, and the gap structure depends on the planet mass, we expect the gravitational stability of planet gaps to also depend on the planet mass. The present study is a natural follow-up to LP12 in which we investigate the role of planet mass.

This paper is organized as follows. In the next subsection, we review the basic properties of the gravitational instability associated with planet gaps, and further explain the motivation for our study. We describe our disc-planet models and numerical methods in §2. We present results for fixed-orbit simulations in §3 and freely-migrating simulations in §4. We show it is possible to for edge modes to counter-act inward migration, but not indefinitely. We find the unstable gap edge easily triggers rapid outward migration. An example of this phenomenon is discussed in §5. We summarize in §6 with a discussion of possible applications of our results to giant planets on wide orbits, and important caveats of our models.

1.1 Gravitational instability of planet gaps

Gaps induced by giant planets are associated with extrema in the disc potential vorticity (PV) profile $\eta = \kappa^2/2\Omega\Sigma$, where κ is the epicycle frequency, Ω is the rotation rate and Σ is the surface density. It is well-known that the presence of PV extrema permits dynamical instability (e.g. Papaloizou & Pringle 1985; Li et al. 2000; Lin & Papaloizou 2010). In the case of a planet gap, local $\max(\eta)$ and local $\min(\eta)$ results from PV generation and destruction across spiral shocks induced by the planet (Koller et al. 2003; Li et al. 2005; Lin & Papaloizou 2010).

The PV profile of a planet gap resembles its Toomre parameter profile $Q = c_s \kappa / \pi G \Sigma$ (Lin & Papaloizou 2011a), where c_s is the sound-speed and G is the gravitational constant. Thus, we may also associate planetary gap instabilities with $\max(Q)$ or $\min(Q)$.

Fig. 1 shows typical Q -profiles for gaps induced by giant planets. Only the outer disc is shown since this is where instability is most prominent in our models. The horizontal axis is plotted in units of Hill radii r_h away from the planet’s orbital radius (defined later). The co-orbital region for massive planets, within which fluid particles execute horseshoe turns upon encountering the planet, is approximately within $2.5r_h$ of the planet’s orbital radius (Artymowicz 2004b; Paardekooper & Papaloizou 2009; Lin & Papaloizou 2010). So the local $\max(Q)$ is located just inside the co-orbital region, while the local $\min(Q)$ is located just outside.

In a self-gravitating disc, Lin & Papaloizou (2011a) showed that there is a gravitational instability associated

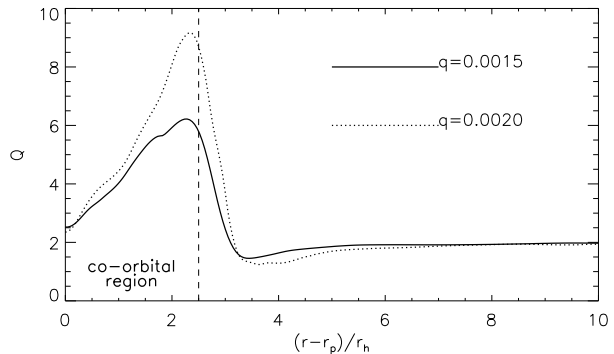


Figure 1. Azimuthally averaged Toomre parameter for gaps opened by planets with different masses (q is the planet-to-star mass ratio). The gap edge spiral instability is associated with the local $\max(Q)$, situated at approximately 2 Hill radii from the planet’s orbital radius. This is to be compared with the co-orbital region of a giant planet, which is approximately $|r - r_p| \lesssim 2.5r_h$ (vertical line). So the instability is associated with a feature *just inside* the gap.

with the local Q -maximum at a planetary gap edge¹. By association we mean that the co-rotation radius r_c of the unstable mode coincides with or is close to that of the PV or Q maximum. The local $\max(Q)$ is situated just inside the gap edge (Fig. 1). Thus, the instability presents non-axisymmetric disturbances in the planet’s co-orbital region. In their disc models where the instability is associated with the outer gap edge, LP12 found the passage of an associated spiral arm leads to a net positive torque applied to the planet, because the spiral arm supplies material to execute inward horseshoe turns upstream of the planet. This interaction is explicitly illustrated in Fig. 8 of LP12.

Fig. 1 shows that the gap profile is a function of planet mass. It is not obvious how this affects the positive torques due to the gap gravitational instability described above. Increasing the planet mass makes the gap edges sharper, which should favour instability and increase spiral mode amplitudes, and lead to stronger torques. On the other hand, a larger planet mass opens a deeper gap with lower surface density (reflected by the larger Q -value in Fig. 1). The latter effect should decrease the magnitude of disc-on-planet torques originating from the co-orbital region.

The purpose of this paper is to clarify, through hydrodynamical numerical experiments, the role of planet mass on the gravitational stability of gaps and the subsequent orbital migration due to the interaction with the instability. Lin & Papaloizou (2011a) found that Saturnian mass planets ultimately migrated inward, despite brief phases of outward migration induced by the gap edge instability. However, LP12 simulated 2-Jupiter mass planets and found sustained outward migration. It is of interest to examine the possibility suggested in LP12: zero net migration due to a balance between the outward migration induced by the instability and the tendency for inward type II migration (Lin & Papaloizou 1986).

¹ See also Meschiari & Laughlin (2008), who originally suggested gravitational instability of planetary gaps based on prescribed disc profiles.

2 DISC-PLANET MODEL

We consider a two-dimensional (2D) gaseous self-gravitating protoplanetary disc of mass M_d orbiting a central star of mass M_* . Embedded within the disc is a planet of mass M_p . We use (r, ϕ) plane polar co-ordinates centered on the star. The disc-planet model is the same as that in LP12, but we describe it here for ease of reference. We adopt units such that $G = M_* = 1$.

The disc has radial extent $r \in [r_i, r_o] = [1, 25]$. The strength of disc self-gravity is characterized by specifying $Q_{k0} \equiv Q_k(r_o)$, where

$$Q_k(r) \equiv \frac{c_{\text{iso}} \Omega_k}{\pi G \Sigma} \quad (1)$$

is the Keplerian Toomre parameter for thin discs. In Eq. 1, c_{iso} is the isothermal sound-speed defined below, $\Omega_k(r) = \sqrt{GM_*/r^3}$ is the Keplerian orbital frequency. For all our simulations, the disc surface density is initialized with $\Sigma(r) \propto r^{-3/2}$ for $r \gg r_i$, such that $Q_{k0} = 1.5$. Our disc model is gravitationally stable to axisymmetric perturbations according to the Toomre criterion (Toomre 1964).

It should be emphasised that the outcome of the simulations depends on the initial Q_{k0} . Our choice of $Q_{k0} = 1.5$ favours the instability-induced outward migration as seen in LP12 (where outward migration slows down for higher Q_{k0} , and is not observed within their simulation timescale of $100P_0$ for $Q_{k0} = 2$). The surface density normalization $Q_{k0} = 1.5$ gives a disc mass of $M_d = 0.08M_*$. This is ~ 8 times larger than the traditional minimum-mass Solar nebula (MMSN, Weidenschilling 1977), but comparable to the more massive MMSN constructed by Desch (2007).

We adopt a locally isothermal equation of state so that the vertically integrated pressure $p = c_s^2 \Sigma$. Without the planet the sound-speed $c_s = c_{\text{iso}} \equiv hr \Omega_k$, where h is the disc aspect-ratio. We fix $h = 0.05$. The sound-speed is modified close to the planet when it is introduced (see §2.1.2). We also impose a constant kinematic viscosity $\nu = 10^{-5} r_i^2 \Omega_k(r_i)$. This corresponds to an alpha-viscosity of order 10^{-3} , which is typical for disc-planet simulations.

2.1 Planet configuration

The main parameter that we vary is the planet mass $M_p \equiv qM_*$, where q is the planet-to-star mass ratio. We consider $q \in [0.3, 3] \times 10^{-3}$, but will be primarily interested in cases with $q \simeq 10^{-3}$. If $M_* = M_\odot$ then $q = 0.001$ corresponds to a Jupiter-mass planet and $q = 0.0003$ corresponds to a Saturn-mass planet. The position of the planet is denoted $\mathbf{r}_p = (r_p, \phi_p)$. The planet is introduced on a circular orbit of radius $r_{p0} = r_p(t = 20P_0) = 10$ where $P_0 = 2\pi/\Omega_k(r_{p0})$. This corresponds to $Q_k(r_{p0}) = 2.77$, and the mass within $|r - r_{p0}| \lesssim 2.5r_h$ is initially $\simeq 10M_p$ for $q = 10^{-3}$.

The planet mass is ramped up from zero to its full value over $10P_0$. Thus the planet is fully introduced into the disc by $t = 30P_0$. Orbital migration is allowed for $t > 30P_0$, if at all. The planet's gravitational potential is softened with a softening length $\epsilon_p = 0.6H$. Accretion onto the planet is neglected, but since we compute the full self-gravity of the gas, material gravitationally bound to the planet effectively increases its mass.

2.1.1 Gap opening criteria

Crida et al. (2006) showed that gap opening by a planet depends specifically on its mass, the disc scale-height $H = hr$, and the viscosity of the disc. Their criterion for gap opening as a function of q , H , and ν is

$$\frac{3}{4} \frac{H}{r_h} + \frac{50}{q} \left(\frac{\nu}{r_p^2 \Omega_p} \right) \lesssim 1, \quad (2)$$

where $r_h = (q/3)^{1/3} r_p$ is the Hill radius of the planet and $\Omega_p \equiv \Omega(r_p)$.

This criteria is useful in determining which of our parameter survey values q , are able to induce a gap in the disc. Specifically, we can solve for the critical gap-opening mass, q_c for which the left-hand side of Eq. 2 equals unity. Doing so, we find that $q_c = 5 \times 10^{-4}$. We therefore expect all planet masses with $q > q_c$ to open gaps. The case with $q = 3 \times 10^{-4}$ is somewhat smaller than q_c , but we will find even a partial gap can be gravitationally unstable.

2.1.2 Equation of state (EOS)

In the presence of the planet, we adopt the following prescription for the sound-speed:

$$c_s = \frac{c_{\text{iso}} h_p d_p}{[(hr)^{7/2} + (h_p d_p)^{7/2}]^{2/7}} \left(1 + \frac{\Omega_{kp}^2}{\Omega_k^2} \right)^{1/2}, \quad (3)$$

where $\Omega_{kp}^2 = GM_p/d_p^3$ with $d_p^2 = |\mathbf{r} - \mathbf{r}_p|^2 + \epsilon_p^2$ and h_p is a dimensionless parameter. Note that $c_s \rightarrow c_{\text{iso}}$ as $d_p \rightarrow \infty$.

Eq. 3 is taken from Pepliński et al. (2008a), and is used here to increase the disc temperature near the planet relative to c_{iso} . The magnitude of this increase is controlled by h_p . This temperature increase mitigates accumulation of gas near $\mathbf{r} = \mathbf{r}_p$. This would occur if we set $c_s = c_{\text{iso}}$ (implying the disc temperature is unaffected by the planet), which may lead to spurious torques arising from gas near the planet due to the diverging potential and limited resolution.

Physically, we expect gas near the planet to heat up as it falls into the planet potential. The appropriate value for h_p depends on detailed thermodynamics occurring near the planet, which would depend on planet mass. However, since use of this EOS in the present study is motivated by numerical considerations, we simply choose h_p to ensure $c_s/c_{\text{iso}} > 1$ everywhere. In practice, we choose $h_p = 0.5$ for all planet masses except for $q = 3 \times 10^{-4}$, for which $h_p = 0.65$ was needed.

2.2 Numerical simulations

We evolve the disc-planet system using the **FARGO** code (Masset 2000; Baruteau & Masset 2008). **FARGO** solves the 2D hydrodynamic equations using a finite-difference scheme similar to the **ZEUS** code (Stone & Norman 1992), except with a modified azimuthal transport algorithm which circumvents the time-step limitation set by the inner disc boundary. The self-gravity solver is described in Baruteau & Masset (2008). When allowed to respond to disc forces, the planet's motion is integrated with a fifth-order Runge-Kutta scheme. Indirect potentials are included to account for the non-inertial reference frame. The disc indi-

rect potential is not expected to play a significant role because our discs are not very massive (cf. Adams et al. 1989; Shu et al. 1990; Kratter et al. 2010a).

The disc is divided into $N_r \times N_\phi$ cells in radius and azimuth, respectively. The radial grid is logarithmically spaced while the azimuthal grid is uniformly spaced. We use $(N_r, N_\phi) = (512, 1024)$ for fixed-orbit simulations (§3) and $(N_r, N_\phi) = (1024, 2048)$ for simulations where the planet is allowed to migrate (§4). In the latter case, the resolution is increased in order to resolve regions close to the planet, where co-orbital torques arise and were found to be responsible for the outward migration seen in LP12.

We then apply open boundaries in the radial direction and periodic boundary conditions in azimuth.

We initialize the disc azimuthal velocity v_ϕ from centrifugal balance with stellar gravity, self-gravity and pressure forces. The initial radial velocity is $v_r = 3\nu/r$.

3 FIXED ORBIT SIMULATIONS

We first examine how the gap edge spiral instability (‘edge modes’ hereafter) and the associated disc-planet torques depend on planet mass. To focus on these issues we neglect orbital migration and hold the planet on a fixed circular orbit throughout the simulations presented in this section.

It is important to keep in mind that fixed-orbit simulations suppress disc-planet torques *due* to orbital migration. Such torques can be expected for giant planets in massive discs undergoing type III migration (Masset & Papaloizou 2003; Peplinski et al. 2008a). Nevertheless, we find these numerical experiments useful to aid the interpretation of freely-migrating cases considered later.

3.1 Gap evolution

Edge modes are associated with local PV maxima located just inside the gap (see Fig. 1). The presence of such instabilities will therefore be reflected in the gap properties such as gap depth. This is a useful quantity to examine because edge modes have a ‘gap-filling’ effect. This signifies material being brought into the co-orbital region of the planet, which can subsequently provide a torque (LP12).

In our disc models the Toomre stability parameter decreases with radius, which favours instability of the outer gap edge rather than the inner gap edge. We therefore focus on the gap structure in $r > r_p$.

Following LP12, we define the radius of the outer gap edge $r_{\text{out}} > r_p$ such that $\delta\Sigma(r_{\text{out}}) = 0$, where

$$\delta\Sigma(r) = \left\langle \frac{\Sigma - \Sigma(t=0)}{\Sigma(t=0)} \right\rangle_\phi \quad (4)$$

is the one-dimensional relative surface density perturbation and $\langle \cdot \rangle_\phi$ denotes azimuthal average. The outer gap depth is defined to be the average value of $\delta\Sigma$ in $r \in [r_p, r_{\text{out}}]$ and is denoted $\langle \delta\Sigma \rangle|_{r_p}^{\text{out}}$. This is a negative quantity because the gap is a surface density deficit, but for convenience we will refer to the magnitude of the outer gap depth simply as the gap depth.

Fig. 2 shows the evolution of the gap depth for a range of planet masses $q \in [0.3, 3.0] \times 10^{-3}$. Increasing q results in

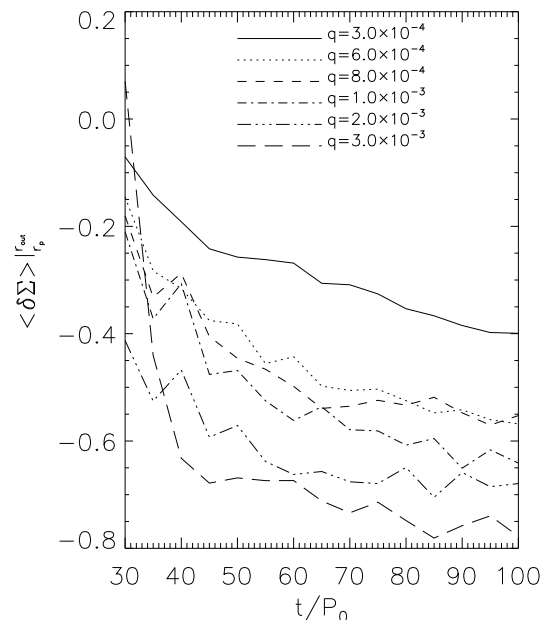


Figure 2. Time evolution of the outer gap depth as a function of planet mass. The gap becomes deeper with time, but the evolution is non-smooth due to the development of edge modes associated with the gap edge. The case with $q = 0.003$ underwent fragmentation, which resulted in a more shallow gap at $t = 30P_0$.

deeper gaps. Local self-gravity is expected to be less important for deeper gaps because the surface density is relatively low compared to $\Sigma(t=0)$. This should discourage gravitational instabilities. However, increasing q produces steeper gap edges which are expected to favour edge modes. In fact, Fig. 2 indicates the latter effect is more important, as discussed below.

An important feature in Fig. 2 is that the gap depth does not decrease monotonically. This signifies instability. In some cases a ‘spike’ appears in the evolution where the gap fills up temporarily, which is attributed to the protrusion of edge mode spiral arms into the gap (LP12, see also Fig. 3). Thus the rate of gap-opening can be slowed down by edge modes. This is explicitly shown in Fig. 2. As a result, the gap is not completely cleared even for $q = 0.002$ ($\delta\Sigma \sim -0.7$) which would be expected if no instabilities develop.

We find edge modes set in earlier with increasing planet mass. The spiral arms develop at $t \sim 50P_0$ for $q = 3 \times 10^{-4}$, which is consistent with previous work (Lin & Papaloizou 2011a). For $q \in [0.6, 2.0] \times 10^{-3}$ the spiral arms develop at $t \sim 40P_0$. An example of the edge modes is shown in Fig. 3.

The instability is also stronger with increasing q . This is reflected in Fig. 2 by the steep increase in $\langle \delta\Sigma \rangle|_{r_p}^{\text{out}}$ at $t \simeq 40P_0$ for $10^3 q = 0.8, 1.0, \text{ and } 2.0$ (the ‘spikes’). By contrast, such gap-filling effect is only just noticeable for $q = 3 \times 10^{-4}$ with a slight decrease in the rate at which the gap deepens around $t \sim 50P_0$ (the small bump), i.e. when instability sets in.

We observed fragmentation in the run with $q = 0.003$. In this case the spiral wake induced by the planet undergoes fragmentation. There is no well-defined gap and

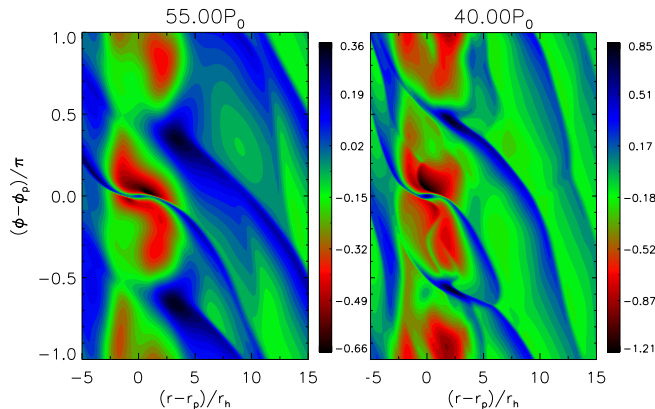


Figure 3. Gravitational instability associated with the gap opened by a Saturnian mass planet ($q = 3 \times 10^{-4}$, left) and a Jovian mass planet ($q = 10^{-3}$, right). The logarithmic surface density perturbation $\log[\Sigma/\Sigma(t=0)]$ is shown. Note that edge modes develop earlier with increasing q .

large-scale coherent edge mode spirals were not identified (cf. Fig. 3). Planet-induced fragmentation of self-gravitating discs have been previously examined by Armitage & Hansen (1999) and Lufkin et al. (2004). We do not consider this fragmenting case further for fixed-orbit or migration simulations.

3.2 Torque measurements

In this section we compare the disc-on-planet torques Γ_{tot} measured from the above simulations. Here, we also apply an exponential envelope to taper off torque contributions from within the planet’s Hill sphere. This avoids potential numerical artifacts from this region because of the low-resolution adopted, and allows us to focus on the effect of edge mode spiral arms, which typically reside in $r \gtrsim r_p + 2r_h$ (LP12).

The previous section showed that edge modes develop earlier and are stronger with Jovian planetary gaps than sub-Jovian gaps. Fig. 4 compares the evolution of the total torque between these two cases. Oscillatory torques signify the presence of edge modes, which occurs almost immediately for $q = 10^{-3}$, but takes longer for $q = 3 \times 10^{-4}$. We also find the average amplitude of the torque oscillations to be larger with increasing planet mass as a consequence of stronger instability. This is despite the fact that increasing q lowers the average surface density in the gap region.

For $q = 3 \times 10^{-4}$, the torque is at first negative due to the planetary wakes (or differential Lindblad torque), until the point at which edge modes develop ($t \sim 50P_0$). The contrast between the torque evolution before and after the onset of instability in Fig. 4 shows that edge modes significantly modify disc-planet torques. That is, the development of edge modes may render the Lindblad torques negligible compared to those provided by the edge mode spirals.

Fig. 4 also shows that the amplitude of the torque oscillations is largest when the instability first sets in (it saturates later). This suggests that in their initial stages of development, edge mode spirals can give the planet a ‘kick’, which can influence the nature of the subsequent orbital migration. However, instantaneous torques in the presence of

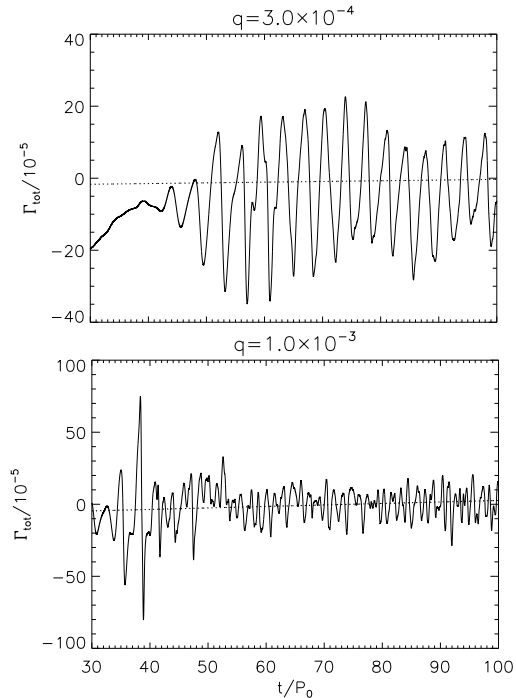


Figure 4. Instantaneous specific disc-on-planet torques, in code units, for $q = 3.0 \times 10^{-4}$ (top) and $q = 10^{-3}$ (bottom). The planet is held on a fixed circular orbit. The straight line in each plot represents a linear fit which indicates the time rate of change in the total torque. Large oscillations signify the development of edge modes, which sets in earlier with increasing q .

edge modes may be positive or negative, so it is difficult to predict the direction of migration based solely on Fig. 4.

It takes $\sim 10P_0$ longer for the $q = 3 \times 10^{-4}$ gap to become unstable than the $q = 10^{-3}$ gap. Although this is a small difference, for giant planets in massive discs considered in this paper, type III migration may be applicable (Masset & Papaloizou 2003), but is suppressed in fixed-orbit simulations. The timescale for type III orbital migration is on the order a few 10’s of P_0 (Pepliński et al. 2008b). This suggests that edge modes may be irrelevant if they do not develop early on, because type III migration could occur before edge modes develop. We confirm this for sub-Jovian planets in §4.

3.2.1 Time-averaged torques

Here, we compute time-averaged torques in order to remove the oscillatory behaviour observed above and compare disc-planet torques for a range of q with unstable gaps. We define the running time-averaged torque as

$$\langle \Gamma_{\text{tot}} \rangle|_{t_0}^t \equiv \frac{1}{t - t_0} \int_{t_0}^t \Gamma_{\text{tot}}(t') dt', \quad (5)$$

and we set $t_0 = 30P_0$. We plot the running time-averaged torque evolution in Fig. 5, while Table 1 compares the values of average torques at the end of the simulation.

Fig. 5 shows that edge modes cause the average torque to become more positive with time. The case with $q = 3 \times 10^{-4}$ has noticeably more negative torque values than cases with larger q . Increasing the planet mass, and hence the

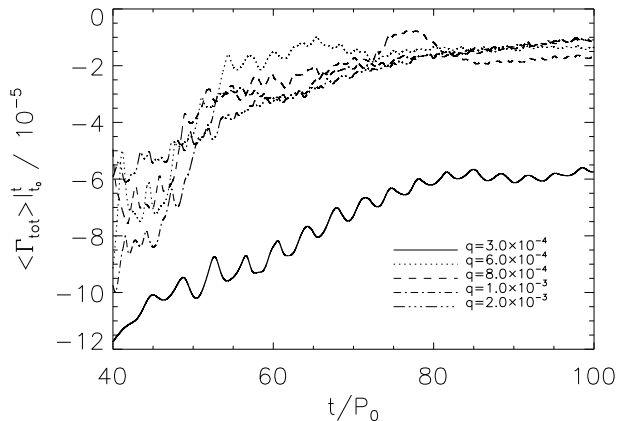


Figure 5. Running time-average specific disc-on-planet torque for a range of planet masses when the gap is unstable to edge modes.

$10^3 q$	$10^5 \langle \Gamma_{\text{tot}} \rangle$
0.3	-5.75
0.6	-1.37
0.8	-1.66
1.0	-1.07
2.0	-1.09

Table 1. The average specific torque acting on each planetary mass (in code units) for fixed-orbit simulations.

instability strength, typically results in more positive disc-on-planet torques (see Table 1). However, the trend is not a clean function of q . This may be due to the fact that increasing planet mass also increases the magnitude of the differential Lindblad torque, which is negative.

3.3 Implications from fixed-orbit simulations

The above numerical experiments show that for the adopted disc parameters, gaps opened by giant planets in self-gravitating discs are unstable to edge modes even for a Saturnian-mass planet ($q = 3 \times 10^{-4}$), which is expected to open a partial gap at most (over sufficiently long timescales). However, edge modes develop later with decreasing q .

The overall effect of increasing q is to increase the strength of the edge mode instability. This is despite the increased tidal torque lowering the gap surface density, an effect that should discourage gravitational instabilities. This effect is, however, outweighed by the increased sharpness of gap edges due to increased q , which favour edge modes.

Given that the edge mode-modified torques oscillate rapidly between positive and negative values, the simulations here cannot be used to predict the direction of orbital migration in the presence of edge modes. Nevertheless, we expect inwards migration to become less favourable with increasing q based on time-averaged torques, which display a more positive torque with increasing planet mass.

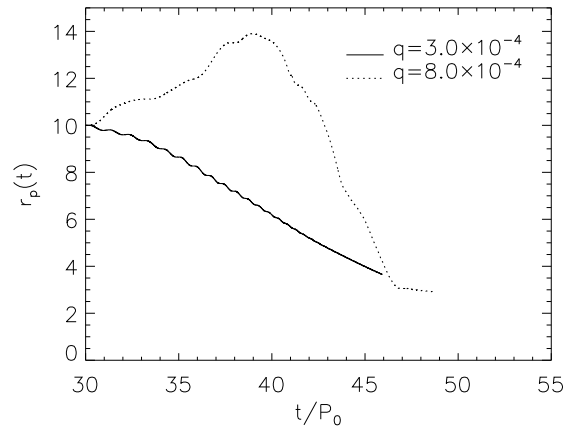


Figure 6. Inward migration of sub-Jovian mass planets in a self-gravitating disc. The case with $q = 3 \times 10^{-4}$ does not develop edge modes at all.

4 SIMULATIONS WITH A FREELY MIGRATING PLANET

In this second set of calculations, we allow the planet to respond to the disc forces after its potential is fully introduced. These simulations permit type III migration, for which the torque results from fluid crossing the planet’s orbital radius and the torque magnitude is proportional to the migration rate (Masset & Papaloizou 2003). Such torques originate close to the planet. Accordingly we double the grid resolution in both directions from the previous experiments (§2.2).

We examine cases with $10^3 q = 0.3, 0.8, 1.0, 1.3, 1.5$ and 2.0. Our specific aim is to see whether or not it is possible to balance the tendency for inward migration with the positive torques induced by the edge modes.

We find the resulting migration is broadly consistent with torque measurements made above. In particular, only planet masses that induce strong instability during gap formation experience the effect of positive torques brought upon them by edge modes. Otherwise, the planet falls in on dynamical timescales.

In fact, only for the cases $q \geq 1.3 \times 10^{-3}$ did we find the situation originally envisioned for our study: a planet residing in a gap with large-scale edge mode spiral arms at the edge over long ($\sim 100P_0$) timescales (such as Fig. 3). We will focus on such cases later, but first briefly review the smaller planet mass runs.

4.1 Inward migration of sub-Jovian mass planets

We find rapid inward migration for planet masses less than about Jovian ($q \lesssim 10^{-3}$). Fig. 6 shows two examples with $q = 3 \times 10^{-4}$ and $q = 8 \times 10^{-4}$.

4.1.1 $q = 3 \times 10^{-4}$

This case undergoes inward migration after release, and falls in within $\sim 15P_0$. This timescale is consistent with type III migration (Masset & Papaloizou 2003; Pepliński et al. 2008b).

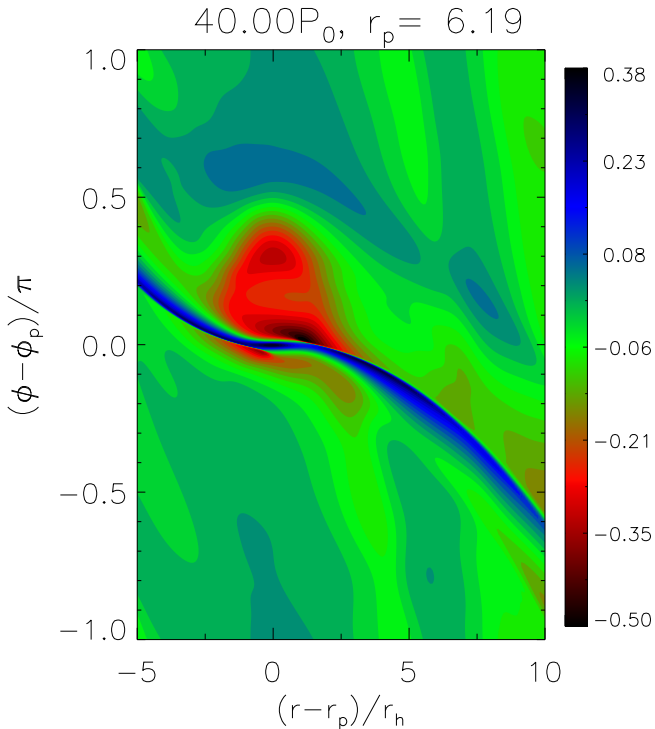


Figure 7. The logarithmic surface density perturbation during inward migration of a planet with $q = 3 \times 10^{-4}$. Notice the surface density excess(deficit) seen behind(ahead of) the azimuthal position of the planet. Such an asymmetry is characteristic of inward type III migration.

The occurrence of type III migration for $q = 3 \times 10^{-4}$ is further evidenced in Fig. 7 where we plot the surface density during the inward migration. The front-back density asymmetry reflects strong co-orbital negative torques originating from fluid crossing the planet’s orbital radius by executing outward horseshoe turns from the inner disc ($r < r_p$) to the outer disc ($r > r_p$) behind the planet ($\phi < \phi_p$).

Note the inward migration timescale for $q = 3 \times 10^{-4}$ is comparable to that needed for edge modes to develop when the planet was held on fixed orbit. However, the planet migrates significantly before a sufficiently deep gap can be opened to induce instability. Therefore edge modes are irrelevant in this case.

4.1.2 $q = 8 \times 10^{-4}$

The orbital evolution for $q = 8 \times 10^{-4}$ displays a more complicated behaviour. In this case we found a disturbance at the outer gap edge has already developed at planet release. It caused the planet to further interact with the outer gap edge, scattering fluid inward, resulting in rapid outward migration on a timescale of $\sim 10P_0$.

Fig. 8 shows snapshots during the initial outward migration. The increase in r_p during this phase is ~ 6 Hill radii (measured at the initial orbital radius of $r = 10$). So the planet is ‘kicked out’ of its original co-orbital region.

However, we find the planet eventually undergoes inward type III migration after reaching a maximum orbital radius of $r \simeq 1.4r_{p0}$. This may be because the edge dis-

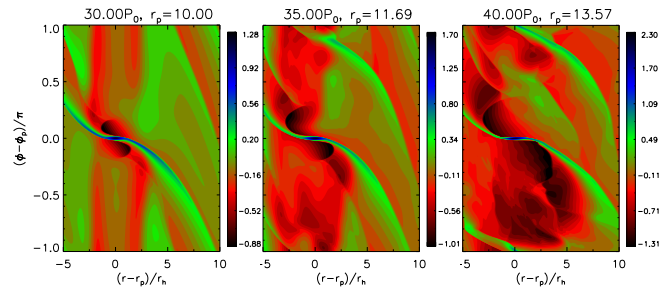


Figure 8. Initial outward migration in the case with $q = 8 \times 10^{-4}$. The logarithmic surface density perturbation is shown. A disturbance at the outer gap edge develops early on, which applies a positive co-orbital torque on the planet (through material executing inward horseshoe turns ahead of the planet).

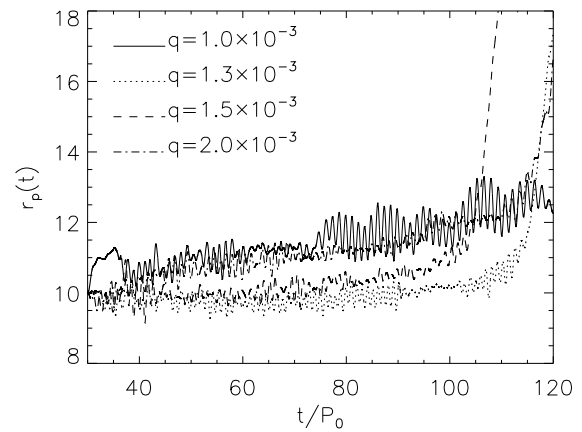


Figure 9. Outward migration of massive planets which open gaps that are unstable to edge modes.

turbance responsible for the initial kick becomes ineffective as the planet has migrated out of its gap. Negative Lindblad torques then initiated inward type III migration. The outward-inward migration seen here is similar to that observed in Lin & Papaloizou (2011a) where a planet scatters off an edge mode spiral arm.

4.2 Outward migration of Jovian planets

We find planet masses with $q \gtrsim 10^{-3}$ induced sufficiently strong edge instabilities early on to counter-act the tendency for inward migration (Specifically to that of inward type III migration as observed for $q = 3 \times 10^{-4}$). Several examples of such cases are shown in Fig. 9. The case with $q = 2 \times 10^{-3}$ was considered in LP12 and is reproduced here for reference (with a longer simulation time). Simulations with $10^3 q = 1.3, 1.5$ were performed to explore the possibility of a torque balance to achieve zero net migration. We see from the figure that this is not possible, and we discuss this issue in more detail later.

Fig. 9 shows that, for $q \geq 0.0013$, orbital migration proceeds, on average, outward more rapidly with increasing planetary mass. The run with $q = 10^{-3}$ does not fit this trend, however. We examine these cases separately below.

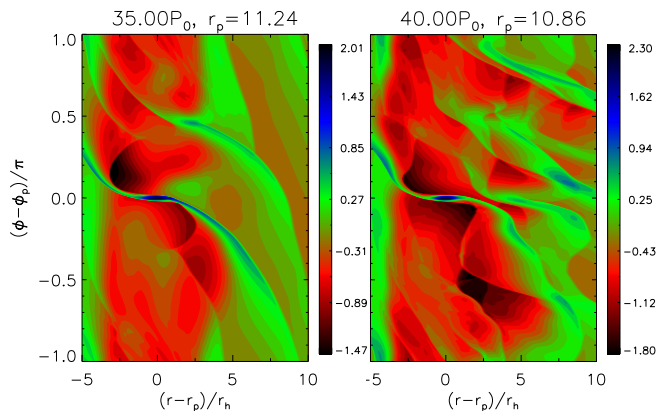


Figure 10. Initial outward migration of the planet with $q = 0.001$ (left) and the disruption of the outer disc afterwards (right).

4.2.1 $q = 10^{-3}$

In this case the planet experiences an initial kick similar to $q = 0.0008$ in the previous section. However, with $q = 0.001$ the initial outward migration in $t = [30, 35]P_0$ corresponds to about 1.4 Hill radii (at $r = 10$), implying the planet remains in its gap afterwards. This is shown in the left panel of Fig. 10. The smaller kick may be due to the increased planet inertia: the fluid mass within the planet’s Hill sphere M_h plus M_p is $0.0017M_*$ for $q = 0.001$ and $0.0012M_*$ for $q = 0.0008$ (at planet release).

The planet, having remained inside the gap, does not experience the rapid inward type III migration observed previously. However, we find the outer disc ($r > r_p$) became highly unstable and dynamic (including transient clumps), as shown in the right panel of Fig. 10. We suspect this is attributable to the passage of the spiral arm upstream of the planet (at $r = r_p + 2.5r_h$ and $\phi - \phi_p = 0.5\pi$) across the planet-induced outer wake.

We did not identify large-scale edge mode spiral arms to persist after the initial outward kick, because it led to a large increase in the effective planet mass ($M_h \sim 0.0037M_*$ by $t = 40P_0$), which strongly perturbs the outer disc directly through the planet-induced wake (becoming unstable itself). The planet nevertheless migrates outwards secularly because the inner gap edge is on average closer to the planet than the outer gap edge.

4.2.2 $q \geq 1.3 \times 10^{-3}$

For these cases, Fig. 9 displays outward migration on two distinct timescales: a relatively slow phase over several 10^3 ’s of P_0 followed by an outward kick towards the end of the simulation.

The mechanism responsible for the first phase was described in LP12. In summary, the passage of outer edge mode spirals by the planet supplies material to execute inward horseshoe turns upstream of the planet. This applies a positive co-orbital torque, and overcomes the negative differential Lindblad torque on average. We find the net outward migration during this phase is roughly linear in time. As Fig. 9 shows, decreasing q and hence instability strength, the migration rate is reduced during this phase. This is de-

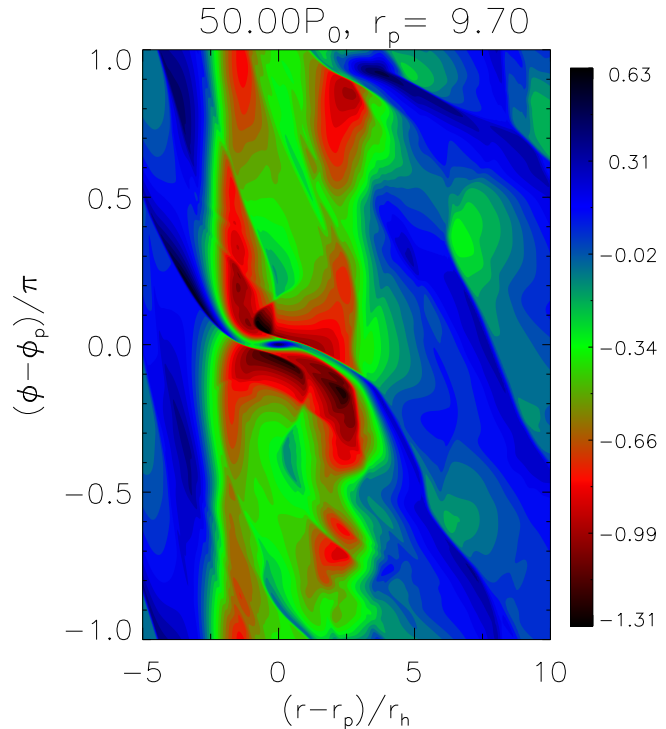


Figure 11. Simulation with a freely migrating planet with mass $q = 0.0013$. This snapshot is taken during the first phase of its migration history when there is a rough balance between the positive torques provided by the outer edge mode spirals and the negative Lindblad torques from the planet-induced wakes (see §4.2.2). However, the planet eventually interacts with the outer disc and is scattered outwards.

spite the expectation that lowering q should permit higher surface densities within the gap.

The second phase of outward migration is very fast and almost monotonic. For $q = 0.002$, r_p increases by about 30% in $t \in [110, 120]P_0$. For $q = 0.0013$ and 0.0015 , r_p increases by more than 60% over a similar timescale. We will examine this phase in more detail in the next section. The extent of outward migration during the second phase is much larger than the initial kicks observed in the previous section with smaller q . We caution that the simulation should not be trusted close to and after $\max(r_p)$ has been attained (i.e. after $t \sim 120P_0$ for $q = 0.0013$), because the planet’s co-orbital region approaches the outer disc boundary.

It is interesting to note that, had we not simulated the case with $q = 0.0013$ beyond $t \simeq 100P_0$, the first phase would suggest little net migration. A snapshot is shown in Fig. 11. However, it still enters the second phase due to interaction with the gap edge as discussed next. Thus, it appears unlikely that a state may be reached in which positive torques due to edge modes balance against the negative differential Lindblad torques, keeping the planet at a fixed orbital radius (which was hypothesized in LP12).

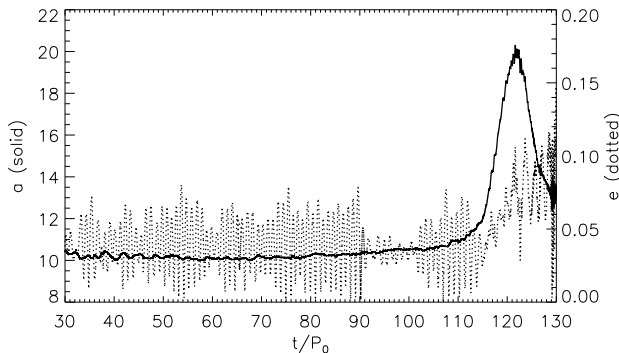


Figure 12. Evolution of semi-major axis a (left, solid) and eccentricity e (right, dotted) for the case with $q = 0.0013$.

5 RAPID OUTWARD TYPE III MIGRATION INDUCED BY EDGE MODES

A common feature in simulations with a freely migrating planet with mass $q \geq 0.0013$ is the second phase of rapid outward migration.

For reference, we show the orbital evolution for $q = 0.0013$ in Fig. 12. The semi-major axis a and eccentricity e were calculated assuming a Keplerian orbit about the central star. The orbit remains fairly circular ($e \lesssim 0.1$) and maintains $a \simeq 10$ for $t \lesssim 80P_0$, but experiences a strong outward kick at $t \sim 100P_0$. This kick appears almost spontaneously. To understand its origin, we examine the fiducial case $q = 0.0013$ in more detail in the proceeding section. This simulation was also performed at a lower resolution ($N_r \times N_\phi = 512 \times 1024$), which exhibited the same qualitative behaviour as the high resolution ($N_r \times N_\phi = 1024 \times 2048$) results discussed here.

We remark that the characteristic kick may also occur in less massive discs. Specifically, we performed low resolution simulations of a $q = 0.0013$ planet migrating in discs with $Q_{k0} = 1.7, 2.0$. In a disc with $Q_{k0} = 1.7$ the planet gets kicked outwards at $t \sim 110P_0$ similar to the fiducial case ($Q_{k0} = 1.5$ at low resolution) but at a slightly later stage in the planet’s evolution. In a disc with $Q_{k0} = 2.0$ the planet remains at $r_p \sim 10$ for the length of the simulation ($t \in [30, 150]P_0$). This is similar to the behaviour of our fiducial case prior to the characteristic kick, which suggests the $q = 0.0013$ planet in the $Q_{k0} = 2.0$ disc may eventually experience the same kick evident in Fig. 12.

5.1 Interaction with the outer gap edge

We first show that the kick is associated with the planet migrating into the outer gap edge. We define the dimensionless outer gap width w_{out} as

$$w_{\text{out}}(t) = \frac{(r_{\text{out}} - r_p)}{r_h}, \quad (6)$$

where we recall r_{out} is the radius of the outer gap edge (§3.1). This definition is only valid when the planet resides in the gap ($w_{\text{out}} > 0$).

The outer gap width leading up to the kick is plotted in Fig. 13, along with $r_p(t)$. For $t \lesssim 110P_0$, w_{out} oscillates on orbital time-scales with an average value of 4. The oscil-

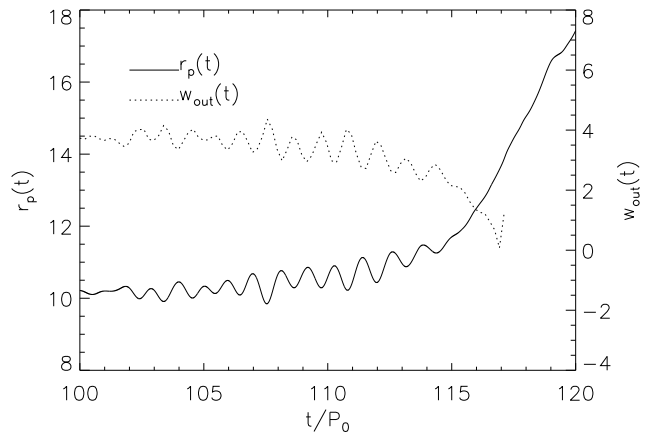


Figure 13. The outer gap width (right, dotted) from $t = 100P_0$ until the planet receives a kick from the unstable gap edge. The planet’s orbital radius r_p is also shown (left, solid). Note that the gap width is undefined when the planet no longer resides in an annular gap, here observed to occur after $t = 117P_0$.

lations are due to the periodic passage of non-axisymmetric over-densities associated with the outer gap edge mode by the planet.

There is a tendency for inward migration due to negative Lindblad torques except when an edge mode spiral is approaching the planet from upstream, by supplying some material to execute inward horseshoe turns. It is evident from the outward migration shown in Fig. 13 that the positive torques supplied by the edge mode spiral overcome negative torques on average. The planet migrates outward with respect to the outer gap edge, so w_{out} decreases.

Notice w_{out} stops oscillating after $t \simeq 115P_0$, and the kick commences. At this point $w_{\text{out}} \simeq 2$. That is, the kick occurs when the outer gap edge enters the co-orbital region of the planet. (Recall the co-orbital region of a giant planet is $|r - r_p| \lesssim 2.5r_h$.) Afterwards r_p rapidly increases and $w_{\text{out}} \rightarrow 0$, implying the planet has exited the gap.

Fig. 14 shows the interaction between the planet and the outer gap edge during this kick. In this case, rather than passing by the planet, the bulk of the edge mode over-density executes an inward horseshoe turn upstream of the planet, i.e. the planet scatters fluid comprising the outer gap edge inwards. The resulting azimuthal surface density asymmetry about the planet is that which characterizes outward type III orbital migration (Pepliński et al. 2008b). An under-dense(over-dense) region behind(ahead of) the planet implies a strong positive co-orbital torque. This configuration persists until the planet migrates close to the outer disc boundary. We conclude that the outer edge mode spiral arms act as a natural ‘trigger’ for outward type III migration.

5.2 Growth of effective planet mass

We also observe a significant increase in the effective planet mass after the planet enters outward type III migration. We define M_ϵ as the fluid mass contained within a radius ϵr_h of the planet. For $\epsilon = 1$, M_ϵ equals M_h defined previously. Note that M_ϵ includes fluid gravitationally bound to the planet

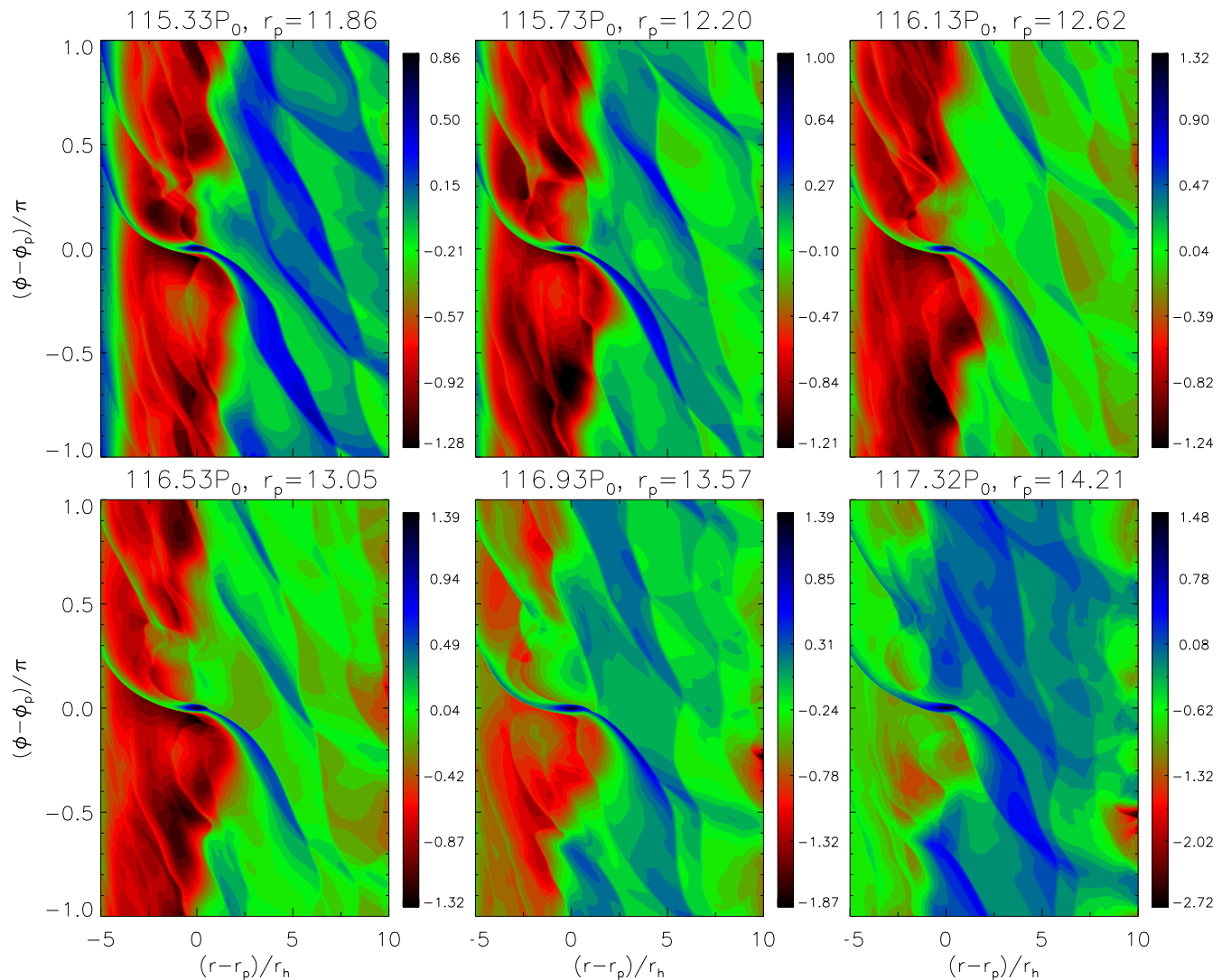


Figure 14. Outward type III migration triggered by an edge mode spiral in the case with $q = 0.0013$. There is relatively little migration for $t \lesssim 100P_0$, but eventually the planet scatters off an edge mode spiral into the outer disc. The logarithmic surface density perturbation is shown.

and orbit-crossing fluid, the latter being responsible for type III migration.

In Fig. 15 we plot M_ϵ/M_p for $\epsilon = 0.3, 0.5$, and 1.0 . For $t \lesssim 110P_0$ there is negligible mass contained within the planet’s Hill radius. This mass rapidly increases as the planet interacts with the edge mode spiral arm ($t \simeq 115P_0$). Notice $M_{\epsilon \geq 0.5}$ increases more rapidly than $M_{\epsilon=0.3}$, suggesting a significant flux of orbit-crossing fluid.

The planet migrates to a maximum orbital radius $\max(r_p) \simeq 18$ at $t \simeq 120P_0$. At this point $M_{\epsilon=0.3} \simeq 0.6M_p$ and the fluid within the Hill radius exceeds the planet mass, $M_h \simeq 1.3M_p$. The rapid increase in planet inertia may attribute to stopping type III migration (Peplinski et al. 2008c). However, since the planet’s co-orbital region approaches the disc boundary ($r_p + 2.5r_h \gtrsim 0.85r_{\text{out}}$), boundary conditions may come into effect (e.g., the lack of disc mass exterior to the planet to sustain type III migration).

Nevertheless, we expect the effective planet mass to generally increase if it undergoes outward type III migration

because the Hill radius r_h scales with orbital radius. In this sense, edge modes can indirectly increase the effective planet mass.

6 SUMMARY AND DISCUSSION

We have performed hydrodynamic simulations of gap-opening satellites (planets) in self-gravitating discs. Our aim was to examine the role of planet mass on the development of gravitational instability associated with the gap, and its subsequent effect on orbital migration.

We first considered simulations where the planet was held on a fixed orbit. Outer gap edge modes developed for planet-to-star mass ratios $q \in [0.3, 2.0] \times 10^{-3}$. Despite being a gravitational instability, we find edge modes developed earlier and are stronger with increasing q , which corresponds to deeper gaps with lower surface density. This is because edge modes are fundamentally associated with potential vorticity maxima resulting from planet-induced

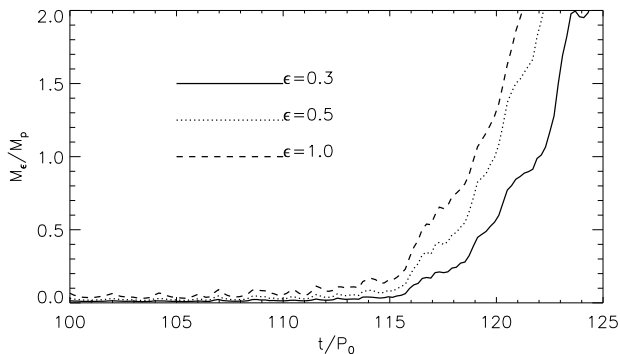


Figure 15. Evolution of fluid mass contained within a fraction ϵ of the planet’s Hill radius in the case with $q = 0.0013$. The time interval corresponds to the planet just prior to and after the interaction with an edge mode spiral arm which scatters it outwards.

spiral shocks, which become sharper with increasing planet mass (Lin & Papaloizou 2010). We also find disc-on-planet torques typically become more positive with increasing q . This is consistent with positive torques being supplied by the outer gap edge mode spirals (LP12).

However, in simulations where orbital migration is allowed, we found edge modes were only relevant for planet masses that opened an unstable gap early on. This is because the condition required for edge modes to develop — a massive disc — also favours type III migration, which operates on dynamical timescales. We found for $q = 0.0003$, the planet immediately underwent inward type III migration, having no time to open a gap.

This initial inward type III migration could be avoided due to initial conditions (Artymowicz 2004a). Pepliński et al. (2008c) demonstrated outward type III migration of giant planets when they are initially placed at the edge of an inner cavity. Thus, an appropriate choice of initial surface density profile may prevent a Saturnian mass planet ($q = 0.0003$) to undergo immediate rapid inward migration as seen in our simulations, and allow it to remain at approximately the same orbital radius for at least ~ 20 orbits. Then edge modes will become relevant, because our fixed-orbit simulations indicate that even the partial gap opened by $q = 0.0003$ is unstable.

For $q \geq 0.0013$ we find net outward migration with an increasing rate with planet mass and therefore gap instability. Although we found it was possible, by decreasing q , to achieve almost zero net migration, this phase only lasted a few 10’s of orbital periods. The planet eventually interacted with an outer gap edge mode spiral and underwent outward type III migration. We conclude that the scenario hypothesized by LP12 — inwards type II migration begin balanced by the positive torques due to outer gap edge mode spirals — is a configuration that is unlikely to persist beyond a few tens of orbital periods.

6.1 Relation to previous studies

Recent hydrodynamic simulations which focus on the orbital migration of giant planets in massive discs have been motivated by the possibility of planet formation through gravitational instability of an initially unstructured disc (Boss

2005, 2013; Baruteau et al. 2011; Michael et al. 2011). Such disc models are already gravitationally unstable without a planet. These studies employed models in which the planet does not significantly perturb the gravito-turbulent disc, and no gap is formed. By contrast, the gravitational instability in our disc model is *caused by* the planet indirectly through gap formation.

Detailed disc fragmentation simulations have shown that, while most clumps formed through gravitational instability are lost from the system (e.g. by rapid inward migration), in some cases it was possible to form a gap-opening clump (Vorobyov & Basu 2010; Vorobyov 2013; Zhu et al. 2012). These authors did not specifically examine gap stability, but we note several interesting results that may hint the presence of edge modes.

In Vorobyov & Basu (2010), a clump is seen to migrate outward. Just prior to this outward migration, their Fig. 1 shows a spiral arm upstream to the planet, and is situated at a radial boundary between low/high disc surface density (but a gap is not yet well-defined). This spiral arm may have contributed to a positive torque on the clump. Their Fig. 1 also suggest an eccentric gap. This is probably due to clump-disc interaction (Papaloizou et al. 2001; Kley & Dirksen 2006; Dunhill et al. 2013), but eccentric gaps have also been observed in disc-planet simulations where edge modes develop and saturate (Lin & Papaloizou 2011a, Fig. 12).

Vorobyov (2013) improved upon Vorobyov & Basu (2010) by including detailed thermodynamics. No edge mode spirals are visible from their plots. However, they found that in all cases where a gap-opening clump is formed, the clump migrates outward. The origin of the required positive torque was not identified. It is conceivable that destruction of the outer gap edge, perhaps due to the edge spiral instability, could result in the clump being on average closer to the inner gap edge than the outer gap edge. This will lead to outwards type II migration.

Zhu et al. (2012) also simulated the fragmentation of massive discs with realistic thermodynamics. In one case where a gap-opening clump formed, further clump formation was observed at the gap edge. The gap-opening clump first migrated outward, but ultimately falls in. This outward migration may be due to the interaction with the unstable gap edge, similar to our simulations.

6.2 Giant planets on wide orbits

Our results have important implications for some models seeking to explain the observation of giant planets on wide orbits. Such examples include the 4 giant planets orbiting HR 8799 between 15–68AU (Marois et al. 2008, 2010), Fomalhaut b at 115AU from its star (Kalas et al. 2008; Currie et al. 2012), and AB Pic b at 260AU (Chauvin et al. 2005).

Disc fragmentation has been proposed as an in situ mechanism to form long-period giant planets (Dodson-Robinson et al. 2009; Boss 2011; Vorobyov 2013). Vorobyov showed that this was possible if the clump opened a gap to avoid rapid inward migration (Baruteau et al. 2011). Then gravitational gap stability becomes an issue that should be addressed. Our results indicate an unstable gap can help to prevent inward migration, but there is the

danger that it may scatter the planet if edge modes persist. The gravitational edge instability is therefore a potential threat to clump survival; in addition to other known difficulties with the disc fragmentation model (see Kratter et al. 2010b).

On the other hand, our simulations reveal a way for a single giant planet to migrate outward, by opening a gravitationally unstable gap and letting it trigger rapid outward type III migration. Our simulations indicate that such outward migration will increase the planet’s effective mass, which may contribute to a circumplanetary disc. Indeed, circumplanetary discs associated with planets on wide orbits have been observed (Bowler et al. 2011). In our models it is not clear whether the rapid increase in effective planet mass discussed in § 5.2 could slow down or halt the triggered rapid outward type III migration. We cannot address this possibility because of the finite disc domain in our models. Conversely, type III migration is self-sustaining (Masset & Papaloizou 2003), so giant planets that underwent type III migration, initiated by this ‘trigger’ mechanism, could be found at large orbital radii.

6.3 Caveats and future work

Our study is subject to several caveats that should be clarified in future work:

Initial conditions. Our simulations with $q = 0.0008$ and $q = 0.001$ displayed very different results for orbital migration, despite having similar planet mass. We identified the planet to interact with a disturbance at the outer gap edge at planet release. This initial kick provided a strong co-orbital torque. It can be interpreted as a brief phase of type III migration, which is known to depend on initial conditions. A more extensive exploration of numerical parameter space is needed to assess the importance of this initial kick. Specifically the resolution of simulations involving these particular planet masses may be important for whether or not the initial interaction between the planet and a disturbance at the outer gap edge occurs.

Thermodynamics. The locally isothermal equation of state implicitly assumes efficient cooling. This favours gap formation and gravitational instabilities. We expect the gap to become gravitationally more stable if the disc is allowed to heat up. Numerical simulations including an energy equation, which adds another parameter to the problem — the cooling time — will be presented in our follow-up paper on the gravitational stability of planet gaps in non-isothermal discs.

Disc geometry. The thin-disc approximation is expected to be valid for gap-opening perturbers, since their Hill radius exceeds the disc thickness by definition. Indeed, three-dimensional (3D) simulations carried out by Lin (2012a) also revealed outward migration of a giant planet due to a gravitationally unstable gap. For partially gap-opening planets (e.g. the $q = 0.0003$ case in our models), 2D works less well, but our simulations indicate they nevertheless open unstable gaps. Whether or not this remains valid in 3D, needs to be addressed.

ACKNOWLEDGMENTS

This project was initiated at the CITA 2012 summer student programme. RC would like to thank CITA for providing funding throughout the project and the use of the Sunnyvale computing cluster. Computations were also performed on the GPC supercomputer at the SciNet HPC Consortium. SciNet is funded by: the Canada Foundation for Innovation under the auspices of Compute Canada; the Government of Ontario; Ontario Research Fund - Research Excellence; and the University of Toronto. The authors thank C. Matzner, K. Kratter and the anonymous referee for comments and suggestions.

REFERENCES

- Adams F. C., Ruden S. P., Shu F. H., 1989, *ApJ*, 347, 959
 Armitage P. J., Hansen B. M. S., 1999, *Nature*, , 402, 633
 Artymowicz P., 2004a, in *Astronomical Society of the Pacific Conference Series*, Vol. 324, *Debris Disks and the Formation of Planets*, L. Caroff, L. J. Moon, D. Backman, & E. Praton, ed., pp. 39–+
 Artymowicz P., 2004b, in *KITP Conference: Planet Formation: Terrestrial and Extra Solar*
 Baruteau C., Masset F., 2008, *ApJ*, 678, 483
 Baruteau C., Masset F., 2013, in *Lecture Notes in Physics*, Berlin Springer Verlag, Vol. 861, *Lecture Notes in Physics*, Berlin Springer Verlag, Souchay J., Mathis S., Tokieda T., eds., p. 201
 Baruteau C., Meru F., Paardekooper S.-J., 2011, *MNRAS*, , 1086
 Boss A. P., 1997, *Science*, 276, 1836
 Boss A. P., 2005, *ApJ*, 629, 535
 Boss A. P., 2011, *ApJ*, 731, 74
 Boss A. P., 2013, *ApJ*, 764, 194
 Bowler B. P., Liu M. C., Kraus A. L., Mann A. W., Ireland M. J., 2011, *ApJ*, 743, 148
 Chauvin G. et al., 2005, *A&A*, 438, L29
 Crida A., Morbidelli A., Masset F., 2006, *Icarus*, 181, 587
 Currie T. et al., 2012, *ApJL*, 760, L32
 Desch S. J., 2007, *ApJ*, 671, 878
 Dodson-Robinson S. E., Veras D., Ford E. B., Beichman C. A., 2009, *ApJ*, 707, 79
 Dong R., Rafikov R. R., Stone J. M., 2011, *ApJ*, 741, 57
 Duffell P. C., MacFadyen A. I., 2013, *ArXiv e-prints*
 Dunhill A. C., Alexander R. D., Armitage P. J., 2013, *MNRAS*, , 428, 3072
 Goldreich P., Tremaine S., 1979, *ApJ*, 233, 857
 Goldreich P., Tremaine S., 1980, *ApJ*, 241, 425
 Kalas P. et al., 2008, *Science*, 322, 1345
 Kley W., Dirksen G., 2006, *A&A*, 447, 369
 Kley W., Nelson R. P., 2012, *ARAA*, 50, 211
 Koller J., Li H., Lin D. N. C., 2003, *ApJL*, 596, L91
 Kratter K. M., Matzner C. D., Krumholz M. R., Klein R. I., 2010a, *ApJ*, 708, 1585
 Kratter K. M., Murray-Clay R. A., Youdin A. N., 2010b, *ApJ*, 710, 1375
 Li H., Finn J. M., Lovelace R. V. E., Colgate S. A., 2000, *ApJ*, 533, 1023
 Li H., Li S., Koller J., Wendroff B. B., Liska R., Orban C. M., Liang E. P. T., Lin D. N. C., 2005, *ApJ*, 624, 1003

- Lin D. N. C., Papaloizou J., 1986, *ApJ*, 309, 846
Lin M.-K., 2012a, PhD thesis, Cambridge University
Lin M.-K., 2012b, *MNRAS*, , 426, 3211
Lin M.-K., Papaloizou J. C. B., 2010, *MNRAS*, , 405, 1473
Lin M.-K., Papaloizou J. C. B., 2011a, *MNRAS*, , 415, 1445
Lin M.-K., Papaloizou J. C. B., 2011b, *MNRAS*, , 415, 1426
Lin M.-K., Papaloizou J. C. B., 2012, *MNRAS*, , 421, 780
Lufkin G., Quinn T., Wadsley J., Stadel J., Governato F., 2004, *MNRAS*, , 347, 421
Marois C., Macintosh B., Barman T., Zuckerman B., Song I., Patience J., Lafrenière D., Doyon R., 2008, *Science*, 322, 1348
Marois C., Zuckerman B., Konopacky Q. M., Macintosh B., Barman T., 2010, *Nature*, , 468, 1080
Masset F., 2000, *A&AS*, , 141, 165
Masset F. S., Papaloizou J. C. B., 2003, *ApJ*, 588, 494
Mayor M., Queloz D., 1995, *Nature*, , 378, 355
Meschiari S., Laughlin G., 2008, *ApJL*, 679, L135
Michael S., Durisen R. H., Boley A. C., 2011, *ApJL*, 737, L42+
Nayakshin S., 2010, *MNRAS*, , 408, L36
Nayakshin S., 2013, *MNRAS*,
Paardekooper S.-J., Papaloizou J. C. B., 2009, *MNRAS*, , 394, 2297
Papaloizou J. C. B., Nelson R. P., Masset F., 2001, *A&A*, 366, 263
Papaloizou J. C. B., Pringle J. E., 1985, *MNRAS*, , 213, 799
Pepliński A., Artymowicz P., Mellema G., 2008a, *MNRAS*, , 386, 164
Pepliński A., Artymowicz P., Mellema G., 2008b, *MNRAS*, , 386, 179
Pepliński A., Artymowicz P., Mellema G., 2008c, *MNRAS*, , 387, 1063
Rafikov R. R., 2002, *ApJ*, 572, 566
Shu F. H., Tremaine S., Adams F. C., Ruden S. P., 1990, *ApJ*, 358, 495
Stone J. M., Norman M. L., 1992, *ApJS*, , 80, 753
Toomre A., 1964, *ApJ*, 139, 1217
Vorobyov E. I., 2013, ArXiv e-prints
Vorobyov E. I., Basu S., 2010, *ApJL*, 714, L133
Weidenschilling S. J., 1977, *APSS*, 51, 153
Zhu Z., Hartmann L., Nelson R. P., Gammie C. F., 2012, *ApJ*, 746, 110